

City University of New York (CUNY)

CUNY Academic Works

Publications and Research

City College of New York

2017

L-2-hydroxyglutarate production arises from non-canonical enzyme function at acidic pH

Andrew M. Intlekofer

Memorial Sloan Kettering Cancer Center

Bo Wang

Memorial Sloan Kettering Cancer Center

Hui Liu

Memorial Sloan Kettering Cancer Center

Hardik Shah

Memorial Sloan Kettering Cancer Center

Carlos Carmona-Fontanie

Memorial Sloan Kettering Cancer Center

See next page for additional authors

[How does access to this work benefit you? Let us know!](#)

More information about this work at: https://academicworks.cuny.edu/cc_pubs/511

Discover additional works at: <https://academicworks.cuny.edu>

This work is made publicly available by the City University of New York (CUNY).

Contact: AcademicWorks@cuny.edu

Authors

Andrew M. Intlekofer, Bo Wang, Hui Liu, Hardik Shah, Carlos Carmona-Fontanie, Ariën S. Rustenburg, Salah Salah, Marilyn R. Gunner, John D. Chodera, Justin R. Cross, and Craig B. Thompson



HHS Public Access

Author manuscript

Nat Chem Biol. Author manuscript; available in PMC 2017 September 06.

Published in final edited form as:

Nat Chem Biol. 2017 May ; 13(5): 494–500. doi:10.1038/nchembio.2307.

L-2-hydroxyglutarate production arises from non-canonical enzyme function at acidic pH

Andrew M. Intlekofer^{1,2}, Bo Wang¹, Hui Liu³, Hardik Shah³, Carlos Carmona-Fontaine⁴, Ariën S. Rustenburg⁴, Salah Salah⁵, M. R. Gunner⁵, John D. Chodera⁴, Justin R. Cross³, and Craig B. Thompson^{1,*}

¹Cancer Biology & Genetics Program, Memorial Sloan Kettering Cancer Center, NY, 10065, USA

²Department of Medicine, Memorial Sloan Kettering Cancer Center, NY, 10065, USA

³The Donald B. and Catherine C. Marron Cancer Metabolism Center, Memorial Sloan Kettering Cancer Center, NY, 10065, USA

⁴Computational Biology Program, Memorial Sloan Kettering Cancer Center, NY, 10065, USA

⁵Physics Department, City College of New York, New York, United States, 10031, USA

Abstract

The metabolite 2-hydroxyglutarate (2HG) can be produced as either a D(R)- or L(S)- enantiomer, each of which inhibits alpha-ketoglutarate (α KG)-dependent enzymes involved in diverse biologic processes. Oncogenic mutations in isocitrate dehydrogenase produce D-2HG, which causes a pathologic blockade in cell differentiation. On the other hand, oxygen limitation leads to accumulation of L-2HG, which can facilitate physiologic adaptation to hypoxic stress in both normal and malignant cells. Here we demonstrate that purified lactate dehydrogenase (LDH) and malate dehydrogenase (MDH) catalyze stereospecific production of L-2HG via ‘promiscuous’ reduction of the alternative substrate α KG. Acidic pH enhances production of L-2HG by promoting a protonated form of α KG that binds to a key residue in the substrate-binding pocket of

Users may view, print, copy, and download text and data-mine the content in such documents, for the purposes of academic research, subject always to the full Conditions of use: http://www.nature.com/authors/editorial_policies/license.html#terms Reprints and permissions information are available online at <http://www.nature.com/reprints/index.html>.

*Address correspondence to Craig B. Thompson, Memorial Sloan Kettering Cancer Center, 1275 York Ave, New York, NY 10065. Phone: 212-639-6561; Fax: 212-717-3299; thompsonc@mskcc.org.

Accession Codes

Referenced Accessions

Protein Data Bank

4OKN: <http://dx.doi.org/10.2210/pdb4okn/pdb>

1110: <http://dx.doi.org/10.2210/pdb1110/pdb>

Author Contributions

A.M.I. and C.B.T. conceived the project, designed the experiments, analyzed the data, and wrote the manuscript. A.M.I. and B.W. performed all of the experiments. H.L., H.S., and J.R.C. assisted with liquid chromatography-mass spectrometry. C.C.-F. assisted with intracellular pH measurement. A.S.R., S.S., M.R.G., and J.D.C. performed the computational modeling. All authors read and approved the manuscript.

Competing Financial Interests

C.B.T. is a founder of Agios Pharmaceuticals and a member of its scientific advisory board. He also serves on the board of directors of Merck and Charles River Laboratories. J.D.C. is a member of the scientific advisory board for Schrödinger, LLC.

Additional Information

Any supplementary information, chemical compound information and source data are available in the online version of the paper.

LDHA. Acid-enhanced production of L-2HG leads to stabilization of hypoxia-inducible factor 1 alpha (HIF-1 α) in normoxia. These findings offer insights into mechanisms whereby microenvironmental factors influence production of metabolites that alter cell fate and function.

Keywords

acidosis; epigenetic; metabolite; microenvironment; oncometabolite; stroma; stem cell; tumor

The discovery of oncogenic mutations in IDH enzymes demonstrated the profound impact that altered metabolism can have on cell identity and function^{1,2}. Mutant IDH enzymes efficiently catalyze reduction of α KG to the 'oncometabolite' D-2HG^{3,4}. D-2HG inhibits a large family of >70 different α KG-dependent enzymes that regulate chromatin-modifications, stability of hypoxia-inducible factors, extracellular matrix maturation, and DNA repair¹. In particular, D-2HG-mediated inhibition of chromatin-modifying enzymes impairs induction of gene expression programs required for normal cell differentiation and 'locks' malignant cells in an undifferentiated stem cell-like state⁵⁻⁷. The relative contributions of different D-2HG targets to oncogenesis likely varies depending on the cellular context^{8,9}.

While intensive efforts have been directed at investigating the molecular and cellular effects of IDH mutant-derived D-2HG, potential sources and functions of the mirror-image enantiomer L-2HG are less well understood¹⁰. Importantly, biochemical assays demonstrated that L-2HG functions as a more potent inhibitor of α KG-dependent enzymes compared to D-2HG; thus cells may be quantitatively more sensitive to changes in L-2HG than D-2HG¹¹⁻¹³. Indeed, deregulated L-2HG disposal causes significant developmental pathology and is associated with brain and kidney cancer¹⁴⁻¹⁶.

It was recently reported that hypoxia induces production of L-2HG by both normal and malignant cells as a physiologic response to oxygen limitation^{17,18}. Hypoxia-induced production of L-2HG occurs independently of HIF but acts to reinforce the hypoxic response, at least in part, through stabilization of HIF protein^{13,17,18}. Accumulation of L-2HG slows glycolysis and mitochondrial respiration by reducing the regeneration of NAD⁺¹⁸. Moreover, hypoxia-induced L-2HG promotes the same repressive chromatin marks that characterize the differentiation blockade of IDH-mutant malignancies^{8,17,19}, consistent with the well established association between hypoxic niches and stem cell populations²⁰.

Genetic evidence suggests that lactate dehydrogenase and malate dehydrogenase enzymes are major sources of hypoxia-induced L-2HG^{16-18,21}, but there has been no demonstration that these enzymes directly catalyze L-2HG production. Here we demonstrate that purified LDH and MDH enzymes can catalyze stereospecific reduction of α KG to L-2HG and that acidic reaction conditions dramatically enhance LDH- and MDH-mediated production of L-2HG *in vitro* and in cells. Mechanistically, acidic pH enhances LDHA-mediated reduction of α KG by driving equilibrium toward a protonated form of α KG that binds more stably to the LDHA enzyme. In living cells, the pH-dependent induction of L-2HG acts as a potent stabilizer of HIF-1 α in normoxia, representing a previously unknown pathway of HIF-1 α stabilization with potential relevance to human disease states. These findings offer new

insights in the mechanisms that regulate non-canonical substrate use by metabolic enzymes and the consequences of promiscuous L-2HG production in cell physiology.

Results

LDH and MDH enzymes use α KG as an alternative substrate

Hypoxic cells undergo a number of metabolic changes (Fig. 1a) including an increased NADH/NAD⁺ ratio^{18,22}, an increased intracellular concentration of α KG^{18,23}, and acidification of the extracellular and intracellular environments^{24,25}. Prior reports implicated lactate dehydrogenase A (LDH) and malate dehydrogenase 1 and 2 (MDH) as contributing to hypoxia-induced L-2HG in cells (Fig. 1a)^{17,18}. To determine if these enzymes could directly produce L-2HG, we tested the ability of purified LDH and MDH to catalyze NADH-dependent reduction of their canonical substrates as well as α KG. As expected, LDH rapidly consumed NADH in the presence of its canonical substrate pyruvate (Fig. 1b). LDH also consumed NADH in the presence of α KG confirming its capacity to utilize alternative larger alpha-ketoacid substrates (Fig. 1b)^{26,27}. Likewise, MDH efficiently catalyzed reduction of its canonical substrate oxaloacetate (Fig. 1c), while also demonstrating an ability to use α KG as a non-canonical substrate, albeit less efficiently (Fig. 1c).

We performed gas chromatography-mass spectrometry (GC-MS) to determine the identities of the alpha-hydroxyacid reaction products generated by LDH and MDH enzymes. Analysis of reaction mixtures without enzyme demonstrated that there was no significant non-enzymatic production of lactate, malate, or 2HG (Fig. 1d–f). LDH, but not MDH, catalyzed reduction of pyruvate to lactate (Fig. 1d). Both MDH and LDH catalyzed reduction of oxaloacetate to malate, with MDH catalyzing this reaction more efficiently than LDH, as expected (Fig. 1e). Notably, both LDH and MDH enzymes were capable of ‘promiscuously’ catalyzing NADH-dependent reduction of the alternative substrate α KG to 2HG (Fig. 1f).

LDH and MDH catalyze reduction of α KG to L-2HG

Standard metabolite derivatization and chromatography methods do not distinguish between enantiomeric species. In order to separate alpha-hydroxyacid enantiomers, we adapted a liquid chromatography-mass spectrometry (LC-MS) protocol involving derivatization of metabolites with the chiral compound diacetyl-L-tartaric anhydride (Supplementary Results, Supplementary Fig. 1)²⁸. The identity of alpha-hydroxyacid enantiomers was confirmed by comparison to similarly derivatized standards (Fig. 2a–c). As expected, chiral derivatization showed that LDH catalyzed reduction of pyruvate to L-lactate, whereas MDH catalyzed this reaction poorly (Fig. 2a). MDH catalyzed its canonical reaction involving reduction of oxaloacetate to L-malate (Fig. 2b), while LDH catalyzed this reaction less effectively (Fig. 2b). Both LDH and MDH catalyzed stereospecific reduction of α KG to L-2HG (Fig. 2c and Supplementary Fig. 2). To ensure that L-2HG production was not facilitated by an unknown contaminant of the enzyme preparations (Supplementary Fig. 3a), we also studied recombinant human LDHA, MDH1, and MDH2 enzymes. The recombinant enzymes also catalyzed stereospecific reduction of α KG to L-2HG (Supplementary Fig. 3b–f).

Collectively, these findings substantiate genetic evidence suggesting that LDH and MDH enzymes contribute to cellular production of L-2HG^{16–18,21}.

Wildtype IDH and PHGDH enzymes produce D-2HG

Prior reports demonstrated that wildtype isocitrate dehydrogenase enzymes can catalyze reduction of α KG to 2HG but the stereochemistry of the 2HG product was not determined^{29,30}. Therefore, we sought to assess whether wildtype IDH enzymes might represent another cellular source of D- or L-2HG. Using a cell-based assay, we observed that transfection with empty vector had no effect on D- or L-2HG levels, whereas transfection with wildtype IDH1 or IDH2 selectively increased D-2HG levels (Supplementary Fig. 4a, b and 5). Supplementation with cell-permeable α KG substrate resulted in a further increase in the amount of D-2HG in cells transfected with wildtype IDH1 or IDH2 (Supplementary Fig. 4a, b and 5), albeit ~50–100 fold less than that observed in cells transfected with an oncogenic IDH1 R132H mutant (Supplementary Fig. 4c).

Commercially available preparations of IDH from porcine heart were impure and thus unsuitable for enzymatic assays, prompting us to use recombinant human IDH1 as an alternative (Supplementary Fig. 3a). Employing previously reported reaction conditions with Tris-based buffers³¹, we detected substantial non-enzymatic production of 2HG that was equally distributed as D- and L- enantiomers (Supplementary Fig. 6). In contrast, non-enzymatic 2HG production was negligible in phosphate-based reaction buffers (Supplementary Fig. 6). Using phosphate-based buffers, we found that recombinant human IDH1 selectively catalyzed production of D-2HG (Supplementary Fig. 4d). Taken together, the cell-based and recombinant enzyme assays demonstrate that wildtype IDH enzymes can catalyze production of D-2HG, an intrinsic enzymatic property that is substantially enhanced by the active site arginine residue mutations in IDH observed in cancer^{29,30}.

The enzyme 3-phosphoglycerate dehydrogenase (PHGDH) was recently identified as another potential cellular source of D-2HG^{32,33}. Indeed, we found that recombinant human PHGDH catalyzed stereospecific reduction of α KG to D-2HG *in vitro* (Supplemental Fig. 4e). The locus encoding PHGDH is frequently amplified in breast cancer and melanoma^{34,35}, and elevated 2HG levels have been detected in primary breast tumors with aggressive features but no IDH mutation³⁶. Thus, determining the chirality of 2HG should help elucidate which metabolic pathway contributes to 2HG production in various cancer settings.

Acidic pH enhances alternative enzymatic activity of LDH

When investigating the enzymatic properties of LDH, we noted a striking enhancement in NADH-dependent reduction of α KG at more acidic pH (Fig. 3a). Specifically, the K_m of LDH for α KG decreased from >15 mM at pH 7.4 to 3.86 ± 0.97 mM at pH 6.0 (Fig. 3c), a value that approximates the concentration of α KG in hypoxic cells¹⁸. We found that the enhanced rate of α KG-dependent NADH consumption at more acidic pH resulted in increased LDH-dependent production of L-2HG (Fig. 3e). Acidification also enhanced the ability of MDH to catalyze reduction of α KG to L-2HG, albeit to a lesser degree (Fig. 3b, d,

f). Although the rate of non-enzymatic NADH degradation increased at acidic pH, there was no detectable non-enzymatic production of L-2HG (Supplementary Fig. 7).

In contrast to the effects on non-canonical substrate usage, acidic pH had no substantial effect on the ability of LDH to reduce its canonical substrate pyruvate at a near physiologic pyruvate concentration of 0.3 mM (Fig. 3g)³⁷. At concentrations of pyruvate greater than 0.3 mM, acidic pH impaired the ability of LDH to reduce pyruvate due to enhanced substrate inhibition as previously described (Fig. 3g, h)³⁸. Together, these results demonstrate that acidification enhances the alternative substrate utilization of lactate dehydrogenase such that the non-canonical substrate α KG is relatively favored at lower pH, resulting in increased production of L-2HG.

We also examined the effects of acidic pH on the ability of wildtype IDH1 and PHGDH to reduce α KG to D-2HG. Wildtype IDH1 exhibited minimal pH-dependent change in D-2HG production (Supplementary Fig. 8a). In contrast, PHGDH exhibited enhancement of D-2HG production in acidic pH (Supplementary Fig. 8b).

Acidity enhances reduction of a subset of alpha-ketoacids

To determine whether acidic pH might increase accessibility to the substrate-binding pocket of LDH, we tested the effect of pH on LDH-mediated reduction of alpha-ketoacids with bulky tail groups, including phenylpyruvate (PP) and hydroxyphenylpyruvate (HPP) (Fig. 4a). We observed that LDH reduced both PP and HPP at a rate at least as great as that of α KG, and there were no substantial pH-dependent changes in the rate of reduction for either substrate (Fig. 4a). These findings suggest that acidic pH does not function merely to enhance access for substrates larger than pyruvate, such as α KG, to the substrate-binding pocket of LDH.

We investigated whether the nature of the chemical moiety present in the tail end of the alpha-ketoacid substrate might dictate the pH-dependent properties of the LDH enzymatic reaction. We identified pairs of alpha-ketoacid substrates of identical carbon-chain length that differed only in whether there was a carboxylate or methyl group present in the final position (Fig. 4b), including oxaloacetate (OAA; 4-carbon), alpha-ketoglutarate (α KG; 5-carbon), and oxoadipic acid (OAdA; 6-carbon) along with their respective methylated counterparts alpha-ketobutyrate (α KB; 4-carbon), oxopentanoic acid (OPA; 5-carbon), and ketohexanoic acid (KHA; 6-carbon). For each substrate pair, only the alpha-ketoacid with a carboxylate group in the final position exhibited pH-dependent enhancement of enzymatic reduction (Fig. 4b).

Acidification enhances interaction of α KG with LDHA Q100

We performed Monte Carlo protonation state modeling simulations with virtually docked substrates to determine whether pH-dependent changes in the protonation states of α KG, NADH, or LDHA might be responsible for the acid-enhanced enzymatic reduction of α KG. The docked structure of α KG demonstrated that the carboxylate group in the tail of the substrate is positioned immediately adjacent to glutamine 100 (Q100) in the substrate-binding pocket of LDHA (Fig. 5a). Prior reports demonstrated that the corresponding residue in bacterial LDH plays an important role in determining substrate specificity^{39,40}.

Analysis of the Monte Carlo simulations demonstrated a change of the predominant protonation state of α KG upon binding LDHA with NADH. The carboxylate tail of α KG has a predicted pK_a of 4.28 ± 1.27 (closely matching the experimental pK_a of 4.4)⁴¹, indicating that it would be mostly deprotonated in solution at pH values ranging from 6.0 to 7.4. However, upon binding to LDHA, the carboxylate tail of α KG becomes protonated whereupon it is predicted to form a hydrogen bond with Q100 (Fig. 5b). This is associated with a free energy penalty for protonating the carboxylate tail that opposes binding, which for a given pH can be expressed as

$$\Delta G_{pH} = k_B T (pH - pK_a) (\ln 10),$$

where k_B is the Boltzmann constant and T equals the absolute temperature. Protonating the carboxylate tail at pH 7.4 would cost $3.2 k_B T$ more than protonating it at pH 6.0 (Fig. 5c). The expected fold change in the aqueous concentration of the deprotonated form is calculated as follows:

$$\frac{e^{-\Delta G_{6.0} / k_B T}}{e^{-\Delta G_{7.4} / k_B T}}$$

If the enzyme greatly prefers to bind the protonated form, then the predicted K_m of α KG would be approximately 25 times higher (lower affinity) at pH 7.4 than at 6.0, absent additional pH-dependent effects. These predictions are consistent with the increased K_m measured experimentally for α KG at pH 7.4 compared to pH 6.0 (Fig. 3c).

Mutation of Q100 to a positively charged amino acid might alter the substrate preference for LDHA, such that it would favor α KG with the carboxylate tail in the deprotonated (negatively charged) state, thus abolishing the pH trend observed with the wildtype LDHA enzyme. Indeed, mutation of the corresponding residue in bacterial LDH from glutamine to arginine (Q102R) enhanced the ability of the enzyme to reduce oxaloacetate^{39,40}. Therefore, we generated vectors expressing either wildtype LDHA (LDHA WT) or LDHA with a point mutation resulting in replacement of glutamine 100 with arginine (LDHA Q100R). The constructs were transfected into 293T cells, and the FLAG-tagged enzymes were purified by immunoprecipitation (Supplementary Fig. 9). Equal quantities of enzyme were used for *in vitro* reactions with NADH cofactor and the substrates alpha-ketoglutarate (α KG), oxopentanoic acid (OPA), pyruvate (Pyr), and oxaloacetate (OAA; Fig. 5d–g).

In contrast to the acid-enhanced reduction of α KG mediated by wildtype LDHA, the LDHA Q100R mutant exhibited a relatively faster rate of α KG reduction at higher pH values with no enhancement of activity as the pH decreased (Fig. 5d). Thus the positive charge of the Q100R appears to eliminate the energetic penalty normally required to protonate the carboxylate tail of α KG. In contrast, the LDHA Q100R mutant exhibited relatively impaired enzymatic reduction of oxopentanoic acid, which has a methyl group in the tail position (Fig. 5f). Likewise, the LDHA Q100R mutant exhibited a relative preference for oxaloacetate (Fig. 5e) and a relatively impaired ability to reduce pyruvate (Fig. 5g). Taken together, these findings suggest that acidic pH enhances the ability of wildtype LDHA to

reduce substrates with a carboxylate group in the final position by diminishing the energetic penalty of protonating the substrate tail to accommodate binding with glutamine 100 in the LDHA substrate-binding pocket. The LDHA Q100R mutant introduces a positively charged residue at the Q100 site, which alters substrate preference such that alpha-ketoacids with carboxylate tails need not pay the energetic cost of being protonated to bind and are relatively favored at higher pH values.

Acid-enhanced production of L-2HG stabilizes HIF-1 α

Given the striking enhancement of LDH-catalyzed L-2HG production observed *in vitro*, we sought to determine the effects of acidification on 2HG production in cells. Cells grown in normoxic conditions were lysed in non-denaturing buffer with pH ranging from 7.5 to 6.0 (Fig. 6a). Cell lysates were used as a source of enzyme for *in vitro* reactions with addition of α KG and NADH, and 2HG production was assessed by GC-MS. As the reaction pH was lowered, there was a progressive increase in the amount of 2HG produced, such that there was >3 fold more 2HG at pH 6.0 compared to pH 7.5 (Fig. 6a). Assessment of chirality by LC-MS confirmed that acidification of cell lysate reactions potently induced production of L-2HG (Fig. 6b). Acid-enhanced L-2HG production was blocked by addition of oxamate, a lactate dehydrogenase inhibitor that is a structural analog of pyruvate (Fig. 6b)⁴². Thus, acid-enhanced production of L-2HG depends, at least in part, on the enzymatic activity of LDH.

Hypoxia results in acidification of the cellular environment and an increase in the intracellular concentration of α KG (Fig. 1a)^{18,23–25}, but it is unclear to what extent these conditions might be sufficient to induce production of L-2HG. Therefore, we tested the effects of acidified medium and/or exogenous α KG on cells cultured in normoxia (Fig. 6c). As previously reported, addition of cell-permeable α KG resulted in a modest increase in 2HG production in cells cultured in standard medium in normoxia (Fig. 6c)¹⁷. However, we observed a synergistic enhancement of 2HG production when cells were cultured in acidified medium supplemented with cell-permeable α KG (Fig. 6c). Quantification of the intracellular concentrations of L- and D-2HG demonstrated that L-2HG levels exceeded 0.3 mM in acidified media supplemented with cell-permeable α KG (Fig. 6d), approximating previous measurements in hypoxic cells^{17,18}. In contrast, D-2HG concentrations were approximately 10 fold lower (Fig. 6d). Measurement of intracellular pH with fluorescent probes demonstrated a value of $\text{pH } 6.53 \pm 0.29$ for cells cultured in acidic medium plus α KG (Supplementary Fig. 10).

Cells cultured in acidic medium plus α KG demonstrated a striking stabilization of HIF-1 α despite the presence of atmospheric oxygen levels (Fig. 6c and Supplementary Fig. 11). The observed stabilization of HIF-1 α by α KG was paradoxical given the fact that α KG functions as substrate for the EGLN enzymes that hydroxylate proline residues on HIF and target it for proteasomal degradation⁴³. Therefore, we examined the effects of acidification plus α KG on the ratio of hydroxyl-HIF-1 α to total HIF-1 α in cells cultured in the presence of the proteasome inhibitor MG132 (Fig. 6e and Supplementary Fig. 11)⁴⁴. Cells cultured in standard medium plus MG132 accumulated hydroxyl-HIF-1 α relative to total HIF-1 α in response to cell-permeable α KG (Fig. 6e and Supplementary Fig. 11). In contrast, cells cultured in acidified medium plus MG132 did not accumulate hydroxyl-HIF-1 α despite a

substantial increase in total HIF-1 α protein (Fig. 6e and Supplementary Fig. 11). Thus, we conclude that acid-enhanced L-2HG production stabilizes HIF-1 α by inhibiting the α KG-dependent prolyl hydroxylases that target HIF-1 α for degradation, in agreement with previously observed effects of L-2HG on prolyl hydroxylases *in vitro*^{11,13}.

To further explore the possibility that acid-enhanced L-2HG lies upstream of HIF-1 α , we tested the effects of ablating LDHA and MDH2, the two enzymes primarily responsible for L-2HG production in cells^{17,18}. Cells treated with non-targeting control siRNA exhibited normoxic stabilization of HIF-1 α when cultured in acidic medium supplemented with α KG (Fig. 6f and Supplementary Fig. 11). Ablation of either LDHA or MDH2 alone partially impaired stabilization of HIF-1 α in response to acidification (Supplementary Fig. 12a, b and 13). However, combined targeting of both LDHA and MDH2 abrogated L-2HG production (Supplementary Fig. 12c) and abolished the ability of cells to stabilize HIF-1 α in response to acidification (Fig. 6f and Supplementary Fig. 11). These findings demonstrate that acid-enhanced conversion of α KG to L-2HG by LDHA and MDH2 is sufficient to stabilize HIF-1 α in the absence of hypoxia.

Discussion

Herein we demonstrate that lactate dehydrogenase and malate dehydrogenase enzymes catalyze ‘promiscuous’ enzymatic reduction of the alternative substrate α KG to L-2HG. Decades-old studies demonstrated alternative substrate use by dehydrogenase enzymes but lacked techniques to accurately assess the identity and chirality of metabolite products^{26,27}. Our findings indicate that there are multiple enzymes that can reduce α KG to 2HG and that the chirality of 2HG is dictated by the specific enzyme involved. For example, LDH and MDH enzymes catalyze stereospecific production of L-2HG, whereas wildtype (and mutant) IDH and PHGDH catalyze stereospecific production of D-2HG.

The findings presented here substantiate prior genetic evidence implicating LDH and MDH as cellular sources of L-2HG^{16–18,21}. In hypoxia, cells selectively produce L-2HG in a manner primarily dependent on LDHA and MDH2^{17,18}. The relative contributions of LDHA and MDH2 to hypoxia-induced L-2HG appear to vary depending on the type of cell, which may be related to enzyme levels and subcellular pools of substrate. Hypoxic cells undergo a variety of metabolic changes that might favor L-2HG production^{18,22–25,45}. Here we identify acidification and increased α KG concentration as factors that are sufficient to induce cellular production of L-2HG in normoxia. Indeed, *in vitro* enzymatic assays demonstrate that the promiscuous enzymatic activity of LDH, and to a lesser extent MDH, is enhanced by acidic pH, resulting in more efficient reduction of α KG to L-2HG. Acidic pH appears to enhance LDHA-mediated reduction of α KG by driving equilibrium toward the protonated state of the carboxylate tail, which permits docking of α KG via interaction with the glutamine 100 in LDHA. Intracellular acidification might also explain, at least in part, the increased L-2HG observed in cells with electron transport chain dysfunction⁴⁶.

In hypoxia, L-2HG can function as a metabolic signaling molecule that mediates physiologic responses to help cells adapt to oxygen limitation^{17,18}. L-2HG acts to stabilize hypoxia-inducible factors by inhibiting the α KG-dependent prolyl hydroxylases that target HIF for

degradation^{11,13}. Whether HIF-1 α stabilization is a qualitatively or quantitatively unique property of L-2HG compared to D-2HG remains controversial^{13,47,48}. We have identified acidosis as previously unappreciated physiologic stimulus that enhances conversion of α KG to L-2HG, resulting in robust stabilization of HIF-1 α in normoxia. HIF-1 α facilitates cellular adaptation to an acid load by inducing expression of carbonic anhydrases⁴⁹, and our findings suggest that acid-enhanced L-2HG may be part of this signaling axis. Indeed, we find that ablation of LDHA and MDH2 abrogates the ability of acidotic cells to stabilize HIF-1 α . It is also possible that acidification and L-2HG cooperate in the stabilization of HIF-1 α ⁵⁰. Compared to L-2HG, we observed approximately 10 fold lower intracellular concentrations of D-2HG. Given that L-2HG functions as a more potent inhibitor of α KG-dependent enzymes than D-2HG¹¹⁻¹³, we conclude that D-2HG derived from wildtype IDH and/or PHGDH is negligible and likely does not play a physiologic role in this setting.

Promiscuous enzymatic activity results in the production of numerous metabolites that have been described as ‘metabolite damage’ or mistakes¹⁰. However, emerging evidence suggests that L-2HG, a metabolite produced by promiscuous enzyme activity, might represent a conserved metabolic response to multiple environmental stimuli including hypoxia and acidosis. L-2HG appears to mediate its effects through both HIF-dependent and HIF-independent mechanisms^{17,18}. Future investigations will be directed at elucidating the mechanisms whereby L-2HG regulates physiologic responses to hypoxia and acidosis, as well as how deregulation of L-2HG metabolism might contribute to oncogenesis^{14,15}.

Online Methods

Reagents

Purified enzymes were purchased from Sigma, including LDH from bovine heart (L2625), LDH from rabbit muscle (L2500), and MDH from porcine heart (M1567). Recombinant human enzymes were purchased from Abcam, including LDHA (ab93699), MDH1 (ab99244), MDH2 (ab99238), IDH1 (ab113858), and PHGDH (ab198455). Substrates, cofactors, and inhibitors were purchased from Sigma, including pyruvate, oxaloacetate, alpha-ketoglutarate, dimethyl-alpha-ketoglutarate, L-lactate, D-lactate, L-malate, D-malate, L-2-hydroxyglutarate, D-2-hydroxyglutarate, alpha-ketobutyrate, oxopentanoic acid, oxoadipic acid, ketohexanoic acid, phenylpyruvate, hydroxyphenylpyruvate, NADH, NADPH, and oxamate. FLAG-tagged wildtype and Q100R mutant LDHA constructs were cloned into the pCDNA3.1(+) vector (Addgene) by standard site-directed mutagenesis and verified by Sanger sequencing.

Cell Culture

Adherent cell lines 293T (purchased from ATCC) and SFXL (SF188 cells with stable expression of Bcl-XL; generated as previously described⁵¹) were maintained at low passage number in high glucose DMEM with 10% FBS, glucose 25 mM, glutamine 4 mM, penicillin 100 units/ml, and streptomycin 100 μ g/ml and split every 2–3 days before reaching confluence. Cell lines were authenticated by Short Tandem Repeat (STR) profiling. Cell lines repeatedly tested negative for mycoplasma throughout the experimental period. For siRNA experiments, cells were reverse-transfected with siRNA mixed with Lipofectamine

RNAiMAX (Life Technologies) in Opti-MEM Reduced Serum Medium (Life Technologies) as described by the manufacturer. The following siRNAs (ThermoFisher) were used: siLDHA = J-008201-06, target sequence: GGCAAAGACUAUAAUGUAA; siMDH2 = J-008439-12, target sequence: CGCCUGACCCUCUAUGAUA. For experiments with acidified medium, standard DMEM was titrated to pH 6.0 at room temperature and atmospheric oxygen then filtered through a sterile 0.2 μm filter prior to use in tissue culture.

Western Blotting

Cell lysates were extracted in 1 \times RIPA buffer (Cell Signaling), sonicated, centrifuged at 21,000 g at 4 $^{\circ}$ C, and supernatants were collected. Nuclear extracts were prepared by harvesting cells in NaCl 50 mM, sucrose 0.5 M, Triton \times 0.5% plus protease/phosphatase inhibitor cocktail (ThermoFisher). Isolated nuclei were washed with KCl 10 mM then lysed in NaCl 500 mM and NP-40 0.1%. Cleared cell lysates or nuclear extracts were quantified by BCA assay (ThermoFisher) and normalized for total protein concentration. Samples were separated by SDS-PAGE, transferred to nitrocellulose membranes (Life Technologies), blocked in 5% milk prepared in Tris buffered saline with 0.1% Tween 20 (TBST), incubated with primary antibodies overnight at 4 $^{\circ}$ C then horseradish peroxidase (HRP)-conjugated secondary antibodies (GE Healthcare; anti-mouse, NA931V, sheep, 1:5000; anti-rabbit, NA934V, donkey, 1:5000) for 1 hr the following day. After incubation with ECL (ThermoFisher or GE Healthcare), imaging was performed using the Amersham Imager 600 (GE Healthcare). Primary antibodies used included: anti-Ezh2 (Cell Signaling, 5246P; rabbit; 1:1000), anti-HIF-1 α (BD Biosciences, 610959; mouse; 1:200), anti-hydroxyl-HIF-1 α (Cell Signaling, 3434P; rabbit; 1:1000), anti-IDH1 (Proteintech, 12332-1-AP; rabbit; 1:1000), anti-IDH2 (Abcam, ab55271; mouse; 1:1000) anti-LDHA (Cell Signaling, 2012S; rabbit; 1:1000), anti-MDH2 (Abcam, ab96193; rabbit; 1:1000), anti-alpha-tubulin (Sigma, T9026; mouse; 1:5000), and anti-vinculin (Abcam, ab18058; mouse; 1:1000).

Intracellular pH Measurement

Cells were loaded with either 5-(and-6)-Carboxy, Acetoxymethyl Ester, Acetate (SNARF-1; Thermo) or 2',7'-Bis-(2-Carboxyethyl)-5-(and-6)-Carboxyfluorescein, Acetoxymethyl Ester (BCECF; Thermo) ratiometric pH probes according to the manufacturer's instructions. After loading with pH probe, cells were incubated in DMEM without phenol red that was either left unmanipulated or titrated to pH 6.0 with addition of either DMSO (vehicle) or dimethyl- α KG 5 mM. After 4 hours of incubation at 37 $^{\circ}$ C with 5% CO₂, fluorescence was measured using a plate reader (Tecan, Infinite M1000). The SNARF-1 probe was detected with a single excitation at 514 nm and a dual-emission ratio (580 nm and 640 nm). The BCECF probe was detected with a dual-excitation (490 nm and 440 nm) and a fixed emission wavelength of 535 nm. Background fluorescence (cells without probes) was subtracted before all calculations. Intracellular pH was quantified by a standard curve ranging from pH 5.5 to pH 7.5 using DMEM with nigericin 10 μM and valinomycin 10 μM to equilibrate intracellular pH with extracellular pH.

Enzyme Assays

Enzyme reactions were conducted in potassium phosphate buffer 33 mM titrated to pH 7.4, 7.0, 6.6, or 6.0. Purified enzymes were used at 5 units/ml, 1 $\mu\text{g/ml}$, or 10 $\mu\text{g/ml}$ as indicated,

and recombinant enzymes were used at 15 $\mu\text{g/ml}$ unless otherwise indicated. FLAG-tagged wildtype and Q100R mutant LDHA enzymes were purified from transfected 293T cells using Anti-FLAG M2 Affinity Gel (Sigma) according to the manufacturer's instructions. FLAG-tagged enzymes were quantified by BCA assay and gel electrophoresis with Coomassie staining. NADH and NADPH were used at 0.22 mM or 0.30 mM respectively throughout unless otherwise indicated. Substrates were used at 1 mM unless otherwise indicated. For NADH consumption assays, reactions were conducted in UV-transparent 96-well plates (Corning) with reaction volumes of 200 μl . A SpectraMax Plus 384 Microplate Reader (Molecular Devices) was used to monitor the absorbance at 340 nm every 30 seconds or 12 seconds throughout the course of the reaction. For each condition, the mean rate of NADH consumption for triplicate control reactions without enzyme was subtracted from the rate of NADH consumption for triplicate experimental reactions with enzyme. Reaction velocities were calculated using an extinction coefficient for NADH at ϵ_{340} of $6220 \text{ M}^{-1} \text{ cm}^{-1}$ and pathlength of 0.56 cm for a 200 μl reaction volume in a standard 96-well plate. For NADH consumption assays with purified LDH and pyruvate, reactions were conducted in UV-transparent 3-ml cuvettes (BrandTech; pathlength 1 cm) with measurement of the absorbance at 340 nm every 2 seconds. For cell lysate enzyme assays, SFXL cells were cultured in normoxic conditions in regular DMEM medium and harvested at subconfluence. The harvested cells were divided into 4 equal fractions, and non-denaturing cell lysates were prepared with PBS plus 0.1% Triton X titrated to pH 7.5, 7.0, 6.5, or 6.0 and used at either 50 or 100 μl per 200 μl reaction with αKG and NADH. The reaction mixtures were stopped after 16 hr, at which time metabolites were extracted, derivatized and analyzed by GC- or LC-MS.

Metabolite Extraction and Analysis

Metabolites were extracted with ice-cold 80:20 methanol:water containing 2 μM deuterated 2-hydroxyglutarate (D-2-hydroxyglutaric-2,3,3,4,4- d_5 acid; deuterated-2HG) as an internal standard. After overnight incubation at -80°C , cell extract was harvested, sonicated, and centrifuged at 21,000 g for 20 min at 4°C to precipitate protein. Extracts were then dried in an evaporator (Genevac EZ-2 Elite). For GC-MS, metabolites were resuspended by addition of 50 μl of methoxyamine hydrochloride (40 mg/ml in pyridine) and incubated at 30°C for 90 min with agitation. Metabolites were further derivatized by addition of 80 μl of MSTFA + 1% TCMS (Thermo Scientific) and 70 μl of ethyl acetate (Sigma) and incubated at 37°C for 30 min. Samples were diluted 1:2 with 200 μl of ethyl acetate, then analyzed using an Agilent 7890A GC coupled to Agilent 5975C mass selective detector. The GC was operated in splitless mode with constant helium carrier gas flow of 1 ml/min and with a HP-5MS column (Agilent Technologies). The injection volume was 1 μl and the GC oven temperature was ramped from 60°C to 290°C over 25 min. Peaks representing compounds of interest were extracted and integrated using MassHunter software (Agilent Technologies) and then normalized to both the internal standard (deuterated-2HG) peak area and protein content as applicable. Ions used for quantification of metabolite levels were 2HG m/z 247 (confirmatory ion m/z 349), deuterated-2HG m/z 252 (confirmatory ion m/z 354), malate m/z 335 (confirmatory ions m/z 233, 245), and lactate m/z 190 (confirmatory ion m/z 219). Peaks were manually inspected and verified relative to known spectra for each metabolite.

For LC-MS, dried samples were derivatized with 100 μ l of freshly prepared 50 mg/ml (+)-diacetyl-L-tartaric anhydride (DATAN, Sigma) in dichloromethane-acetic acid (v/v=4:1) at 75° C for 30 min. After cooling to room temperature, derivatized samples were dried under nitrogen at room temperature and resuspended in 200 μ l of UltraPure water (18.2 M Ω , PureLab) prior to LC-MS/MS analysis. Analysis was performed on a Thermo Vantage triple-quadrupole mass spectrometer operating in SRM and negative ionization modes. LC separation was using an Acquity UPLC HSS T3 analytical column (2.1 \times 100 mm, 1.8 μ m, Waters) with an Agilent 1260 infinity binary pump. Mobile phase A was 125 mg/l ammonium formate in water adjusted to pH 3.5 with formic acid, mobile phase B was methanol, and flow rate was 0.3 ml/min. Initial conditions were 3% B for 5 min, then increased to 80% B at 5.5 min and held for a further 2.5 min. 10 min of re-equilibration time was used to ensure retention time stability. The column temperature was held at 40° C. Samples were kept at 4° C and the injection volume was 5 μ l. MS source parameters were spray voltage: 2500 V; capillary temperature: 300° C; vaporizer temperature: 250° C; sheath gas pressure: 50 psi; aux gas pressure: 40 psi. Compound specific S-lens values were: 37 V (2HG), 36 V (malate), 34 V (lactate), 40 V (α -ketoglutarate), and 41 V (deuterated-2HG). Individual reactions monitored and collision energies (CE) were: 2HG m/z 363.0 \rightarrow 147.1 (CE: 12 V)*, 129.1 (CE: 27 V); malate m/z 349.0 \rightarrow 133.0 (CE 14 V)*, 115.0 (CE 28 V); lactate m/z 305.0 \rightarrow 89.1 (CE 14 V)*, α -ketoglutarate m/z 145.1 \rightarrow 57.0 (CE 12 V); 113.0 (CE 16V); deuterated-2HG m/z 368.0 \rightarrow 152.1 (CE 13 V)*, 132.9 (CE 22 V), with * indicating the primary transition used to quantify each metabolite. Pure standards of L-2HG, D-2HG, L-malate, D-malate, L-lactate, and D-lactate were derivatized and analyzed in parallel for each chiral determination experiment. The identities of metabolite enantiomers were determined by comparing to the retention times of the derivatized pure standards and additionally confirmed by spike-ins of derivatized pure standards into the experimental sample. Absolute metabolite quantitation was performed using an external calibration curve with deuterated-2HG internal standard and the resulting concentrations corrected for the total cell volume extracted. Chromatograms were acquired and processed with XCalibur and TraceFinder software (ThermoFisher).

Aqueous solution pK_a prediction

The aqueous solution pK_a values for the tail carboxylate moiety of α KG were predicted using Epik (Schrödinger Release 2015-3)⁵² using default settings.

Virtual docking of α KG to LDHA

Virtual docking of α KG was performed using Glide XP (Schrödinger release 2015-3)^{53,54} to chain A of the 2.1 Å structure of lactate dehydrogenase A (LDHA pdb identifier: 4OKN⁵⁵). Missing side chains were automatically constructed, amino acids were assigned protonation states compatible with a pH of 7.0 using the protein preparation wizard (Schrödinger release 2015-3), and crystallographic waters were removed. Bond orders for NADH were manually verified to avoid misassignment. Oxalate was used as a reference ligand to define the binding site, after adding fictitious atoms to ensure minimum atom requirement for binding site definition was met. Hydroxyl and thiol groups were allowed to rotate during grid generation. The tail-protonated form of α KG was docked in the presence of crystallographic NADH. Docking poses were minimized post-docking. The resulting conformations were

clustered within a 0.5 Å RMSD cutoff. This resulted in a single representative pose. All steps utilized default parameters unless otherwise noted. Poses and predicted hydrogen bonds were visualized using PyMOL.

Monte Carlo protonation state modeling using MCCE2 simulations

MCCE2⁵⁶ was used to perform Monte Carlo simulations of amino acid side chain position and side chain and substrate protonation at equilibrium. The 2.3 Å structure of lactate dehydrogenase A (LDHA pdb identifier: 1I10⁵⁷) was used as input for all calculations (~60 computational hours at two Intel® Xeon™ 2.40 GHz Six Core CPU). αKG was modeled using a virtually docked pose from previous work¹⁷. This structure was prepared using the same docking procedure as detailed in this paper. The protonation states were compared between structures with the coenzyme and substrate (NADH and αKG) bound to LDHA or removed. The same starting protein structure was used for both bound and unbound types of simulation. The simulations were performed between pH 4.0–10.0 at intervals of 1.0 pH unit, and at pH 6.6 and 7.4. The total number of MC steps for the equilibration at each pH was 480000. MCCE2 explores all side chain rotamers. DelPhi⁵⁸ was used to solve the Poisson Boltzmann equation to obtain the pairwise interactions between charged and/or polar groups and the solvation energy with an internal dielectric constant of 4.0 and 80 for the solvent, with 0.15 salt concentration. The atomic partial charges and radii for the amino acids were obtained from PARSE⁵⁹, while those of the ligands were generated by QUACPAC (Openeye toolkit 2016-Jun.1). MCCE2 calculates how the protein modifies the solution pK_a (pK_{a,sol}) of amino acids and substrates upon transfer into its position in the protein. NADH, and αKG protonation states and tautomers, including their relative populations were generated and performed using Epik (Schrödinger Release 2015-3). Relative Epik energies were calculated at pH 4.0–10.0 at intervals of 1.0 pH unit, pH 6.6 and pH 7.4. The energetic description for amino acids or standard ligands includes the pK_{a,sol} as well as AMBER⁶⁰ torsion energies and van der Waals self-interactions. For the substrate, values were set to zero and the relative Epik energy of each tautomer and protonation state provided the starting reference state in solution. MCCE2 then calculated the shift in relative energy within the protein and thus showed the change in their distribution. The protein side chain rotamers and protonation states were sampled along with the ligand tautomers and protonation states at the given pH.

Data availability

The docking and MCCE2 calculation data, including scripts, have been deposited in “figshare” (<https://dx.doi.org/10.6084/m9.figshare.4289894.v3>). Inside the zip file, see the ‘Docking’ folder for files used in the docking procedures. Docking was performed using Maestro as part of Schrodinger release 2015-3. See the ‘MCCE’ folder for files used for the MCCE2 calculations for lactate dehydrogenase A. MCCE calculations were performed using MCCE2 (<https://sites.google.com/site/mccewiki/install-mcce>). Epik calculations were performed using Schrodinger release 2015-3.

Supplementary Material

Refer to Web version on PubMed Central for supplementary material.

Acknowledgments

We thank members of the Thompson laboratory for helpful discussions. We thank Mehtap Isik, Sonya Hanson, and Andrea Rizzi from the Chodera laboratory for assistance. A.M.I. was supported by the NIH/NCI (K08 CA201483-01A1), Leukemia & Lymphoma Society (Special Fellow Award 3356-16), Burroughs Wellcome Fund (Career Award for Medical Scientists 1015584), Conquer Cancer Foundation of ASCO, Susan and Peter Solomon Divisional Genomics Program, and Steven A. Greenberg Fund. The work was also supported, in part, by the Leukemia & Lymphoma Society Specialized Center of Research Program (7011-16), the Starr Cancer Consortium (I6-A616), and grants from the NIH, including R01 CA168802-02 (C.B.T.), K99 CA191021-01A1 (C.C.-F.), and the Memorial Sloan Kettering Cancer Center Support Grant (NIH P30 CA008748). M.R.G. and S.S. received financial support from the National Science Foundation (MCB 1022208) and infrastructure support from the National Institute on Minority Health and Health Disparities (8G12MD007603-29).

References

1. Losman JA, Kaelin WG Jr. What a difference a hydroxyl makes: mutant IDH, (R)-2-hydroxyglutarate, and cancer. *Genes Dev.* 2013; 27:836–52. [PubMed: 23630074]
2. Pavlova NN, Thompson CB. The Emerging Hallmarks of Cancer Metabolism. *Cell Metab.* 2016; 23:27–47. [PubMed: 26771115]
3. Dang L, et al. Cancer-associated IDH1 mutations produce 2-hydroxyglutarate. *Nature.* 2009; 462:739–44. [PubMed: 19935646]
4. Ward PS, et al. The common feature of leukemia-associated IDH1 and IDH2 mutations is a neomorphic enzyme activity converting alpha-ketoglutarate to 2-hydroxyglutarate. *Cancer Cell.* 2010; 17:225–34. [PubMed: 20171147]
5. Figueroa ME, et al. Leukemic IDH1 and IDH2 mutations result in a hypermethylation phenotype, disrupt TET2 function, and impair hematopoietic differentiation. *Cancer Cell.* 2010; 18:553–67. [PubMed: 21130701]
6. Lu C, et al. IDH mutation impairs histone demethylation and results in a block to cell differentiation. *Nature.* 2012; 483:474–8. [PubMed: 22343901]
7. Sasaki M, et al. IDH1(R132H) mutation increases murine haematopoietic progenitors and alters epigenetics. *Nature.* 2012; 488:656–9. [PubMed: 22763442]
8. Kats LM, et al. Proto-oncogenic role of mutant IDH2 in leukemia initiation and maintenance. *Cell Stem Cell.* 2014; 14:329–41. [PubMed: 24440599]
9. Saha SK, et al. Mutant IDH inhibits HNF-4alpha to block hepatocyte differentiation and promote biliary cancer. *Nature.* 2014; 513:110–4. [PubMed: 25043045]
10. Linster CL, Van Schaftingen E, Hanson AD. Metabolite damage and its repair or pre-emption. *Nat Chem Biol.* 2013; 9:72–80. [PubMed: 23334546]
11. Chowdhury R, et al. The oncometabolite 2-hydroxyglutarate inhibits histone lysine demethylases. *EMBO Rep.* 2011; 12:463–9. [PubMed: 21460794]
12. Xu W, et al. Oncometabolite 2-hydroxyglutarate is a competitive inhibitor of alpha-ketoglutarate-dependent dioxygenases. *Cancer Cell.* 2011; 19:17–30. [PubMed: 21251613]
13. Koivunen P, et al. Transformation by the (R)-enantiomer of 2-hydroxyglutarate linked to EGLN activation. *Nature.* 2012; 483:484–8. [PubMed: 22343896]
14. Haliloglu G, et al. L-2-hydroxyglutaric aciduria and brain tumors in children with mutations in the L2HGDH gene: neuroimaging findings. *Neuropediatrics.* 2008; 39:119–22. [PubMed: 18671189]
15. Shim EH, et al. L-2-Hydroxyglutarate: An Epigenetic Modifier and Putative Oncometabolite in Renal Cancer. *Cancer Discov.* 2014; 4:1290–8. [PubMed: 25182153]
16. Rzem R, et al. A mouse model of L-2-hydroxyglutaric aciduria, a disorder of metabolite repair. *PLoS One.* 2015; 10:e0119540. [PubMed: 25763823]
17. Intlekofer AM, et al. Hypoxia Induces Production of L-2-Hydroxyglutarate. *Cell Metab.* 2015; 22:304–11. [PubMed: 26212717]
18. Oldham WM, Clish CB, Yang Y, Loscalzo J. Hypoxia-Mediated Increases in L-2-hydroxyglutarate Coordinate the Metabolic Response to Reductive Stress. *Cell Metab.* 2015; 22:291–303. [PubMed: 26212716]

19. Chen C, et al. Cancer-associated IDH2 mutants drive an acute myeloid leukemia that is susceptible to Brd4 inhibition. *Genes Dev.* 2013; 27:1974–85. [PubMed: 24065765]
20. Simon MC, Keith B. The role of oxygen availability in embryonic development and stem cell function. *Nat Rev Mol Cell Biol.* 2008; 9:285–96. [PubMed: 18285802]
21. Rzem R, Vincent MF, Van Schaftingen E, Veiga-da-Cunha M. L-2-hydroxyglutaric aciduria, a defect of metabolite repair. *J Inherit Metab Dis.* 2007; 30:681–9. [PubMed: 17603759]
22. Garofalo O, Cox DW, Bachelard HS. Brain levels of NADH and NAD⁺ under hypoxic and hypoglycaemic conditions in vitro. *J Neurochem.* 1988; 51:172–6. [PubMed: 3379400]
23. Wise DR, et al. Hypoxia promotes isocitrate dehydrogenase-dependent carboxylation of alpha-ketoglutarate to citrate to support cell growth and viability. *Proc Natl Acad Sci U S A.* 2011; 108:19611–6. [PubMed: 22106302]
24. Bright CM, Ellis D. Intracellular pH changes induced by hypoxia and anoxia in isolated sheep heart Purkinje fibres. *Exp Physiol.* 1992; 77:165–75. [PubMed: 1311938]
25. Yan GX, Kleber AG. Changes in extracellular and intracellular pH in ischemic rabbit papillary muscle. *Circ Res.* 1992; 71:460–70. [PubMed: 1628400]
26. Meister A. Reduction of alpha gamma-diketo and alpha-keto acids catalyzed by muscle preparations and by crystalline lactic dehydrogenase. *J Biol Chem.* 1950; 184:117–29. [PubMed: 15421980]
27. Schatz L, Segal HL. Reduction of alpha-ketoglutarate by homogeneous lactic dehydrogenase X of testicular tissue. *J Biol Chem.* 1969; 244:4393–7. [PubMed: 4308858]
28. Struys EA, Jansen EE, Verhoeven NM, Jakobs C. Measurement of urinary D- and L-2-hydroxyglutarate enantiomers by stable-isotope-dilution liquid chromatography-tandem mass spectrometry after derivatization with diacetyl-L-tartaric anhydride. *Clin Chem.* 2004; 50:1391–5. [PubMed: 15166110]
29. Pietrak B, et al. A tale of two subunits: how the neomorphic R132H IDH1 mutation enhances production of alphaHG. *Biochemistry.* 2011; 50:4804–12. [PubMed: 21524095]
30. Rendina AR, et al. Mutant IDH1 enhances the production of 2-hydroxyglutarate due to its kinetic mechanism. *Biochemistry.* 2013; 52:4563–77. [PubMed: 23731180]
31. Leonardi R, Subramanian C, Jackowski S, Rock CO. Cancer-associated isocitrate dehydrogenase mutations inactivate NADPH-dependent reductive carboxylation. *J Biol Chem.* 2012; 287:14615–20. [PubMed: 22442146]
32. Fan J, et al. Human phosphoglycerate dehydrogenase produces the oncometabolite D-2-hydroxyglutarate. *ACS Chem Biol.* 2015; 10:510–6. [PubMed: 25406093]
33. Mattaini KR, et al. An epitope tag alters phosphoglycerate dehydrogenase structure and impairs ability to support cell proliferation. *Cancer Metab.* 2015; 3:5. [PubMed: 25926973]
34. Locasale JW, et al. Phosphoglycerate dehydrogenase diverts glycolytic flux and contributes to oncogenesis. *Nat Genet.* 2011; 43:869–74. [PubMed: 21804546]
35. Possemato R, et al. Functional genomics reveal that the serine synthesis pathway is essential in breast cancer. *Nature.* 2011; 476:346–50. [PubMed: 21760589]
36. Terunuma A, et al. MYC-driven accumulation of 2-hydroxyglutarate is associated with breast cancer prognosis. *J Clin Invest.* 2014; 124:398–412. [PubMed: 24316975]
37. Zhu A, Romero R, Petty HR. A sensitive fluorimetric assay for pyruvate. *Anal Biochem.* 2010; 396:146–51. [PubMed: 19748474]
38. Vesell ES. pH dependence of lactate dehydrogenase isozyme inhibition by substrate. *Nature.* 1966; 210:421–2. [PubMed: 5963238]
39. Wilks HM, et al. A specific, highly active malate dehydrogenase by redesign of a lactate dehydrogenase framework. *Science.* 1988; 242:1541–4. [PubMed: 3201242]
40. Dunn CR, et al. Design and synthesis of new enzymes based on the lactate dehydrogenase framework. *Philos Trans R Soc Lond B Biol Sci.* 1991; 332:177–84. [PubMed: 1678537]
41. Tokonami N, et al. alpha-Ketoglutarate regulates acid-base balance through an intrarenal paracrine mechanism. *J Clin Invest.* 2013; 123:3166–71. [PubMed: 23934124]
42. Novoa WB, Winer AD, Glaid AJ, Schwert GW. Lactic dehydrogenase. V. Inhibition by oxamate and by oxalate. *J Biol Chem.* 1959; 234:1143–8. [PubMed: 13654335]

43. Schofield CJ, Ratcliffe PJ. Oxygen sensing by HIF hydroxylases. *Nat Rev Mol Cell Biol.* 2004; 5:343–54. [PubMed: 15122348]
44. Finley LW, et al. SIRT3 opposes reprogramming of cancer cell metabolism through HIF1alpha destabilization. *Cancer Cell.* 2011; 19:416–28. [PubMed: 21397863]
45. Metallo CM, et al. Reductive glutamine metabolism by IDH1 mediates lipogenesis under hypoxia. *Nature.* 2012; 481:380–4.
46. Mullen AR, et al. Oxidation of alpha-ketoglutarate is required for reductive carboxylation in cancer cells with mitochondrial defects. *Cell Rep.* 2014; 7:1679–90. [PubMed: 24857658]
47. Zhao S, et al. Glioma-derived mutations in IDH1 dominantly inhibit IDH1 catalytic activity and induce HIF-1alpha. *Science.* 2009; 324:261–5. [PubMed: 19359588]
48. Tarhonskaya H, et al. Non-enzymatic chemistry enables 2-hydroxyglutarate-mediated activation of 2-oxoglutarate oxygenases. *Nat Commun.* 2014; 5:3423. [PubMed: 24594748]
49. Chiche J, et al. Hypoxia-inducible carbonic anhydrase IX and XII promote tumor cell growth by counteracting acidosis through the regulation of the intracellular pH. *Cancer Res.* 2009; 69:358–68. [PubMed: 19118021]
50. Mekhail K, Gunaratnam L, Bonicalzi ME, Lee S. HIF activation by pH-dependent nucleolar sequestration of VHL. *Nat Cell Biol.* 2004; 6:642–7. [PubMed: 15181450]
51. Wise DR, et al. Myc regulates a transcriptional program that stimulates mitochondrial glutaminolysis and leads to glutamine addiction. *Proc Natl Acad Sci U S A.* 2008; 105:18782–7. [PubMed: 19033189]
52. Shelley JC, et al. Epik: a software program for pK(a) prediction and protonation state generation for drug-like molecules. *J Comput Aided Mol Des.* 2007; 21:681–91. [PubMed: 17899391]
53. Friesner RA, et al. Glide: a new approach for rapid, accurate docking and scoring. 1. Method and assessment of docking accuracy. *J Med Chem.* 2004; 47:1739–49. [PubMed: 15027865]
54. Halgren TA, et al. Glide: a new approach for rapid, accurate docking and scoring. 2. Enrichment factors in database screening. *J Med Chem.* 2004; 47:1750–9. [PubMed: 15027866]
55. Kolappan S, et al. Structures of lactate dehydrogenase A (LDHA) in apo, ternary and inhibitor-bound forms. *Acta Crystallogr D Biol Crystallogr.* 2015; 71:185–95. [PubMed: 25664730]
56. Song Y, Mao J, Gunner MR. MCCE2: improving protein pKa calculations with extensive side chain rotamer sampling. *J Comput Chem.* 2009; 30:2231–47. [PubMed: 19274707]
57. Read JA, Winter VJ, Eszes CM, Sessions RB, Brady RL. Structural basis for altered activity of M- and H-isozyme forms of human lactate dehydrogenase. *Proteins.* 2001; 43:175–85. [PubMed: 11276087]
58. Yang AS, Gunner MR, Sampogna R, Sharp K, Honig B. On the calculation of pKas in proteins. *Proteins.* 1993; 15:252–65. [PubMed: 7681210]
59. Cornell WD, et al. A second generation force field for the simulation of proteins, nucleic acids, and organic molecules (vol 117, pg 5179, 1995). *Journal of the American Chemical Society.* 1996; 118:2309–2309.
60. Levitt M, Lifson S. Refinement of protein conformations using a macromolecular energy minimization procedure. *J Mol Biol.* 1969; 46:269–79. [PubMed: 5360040]

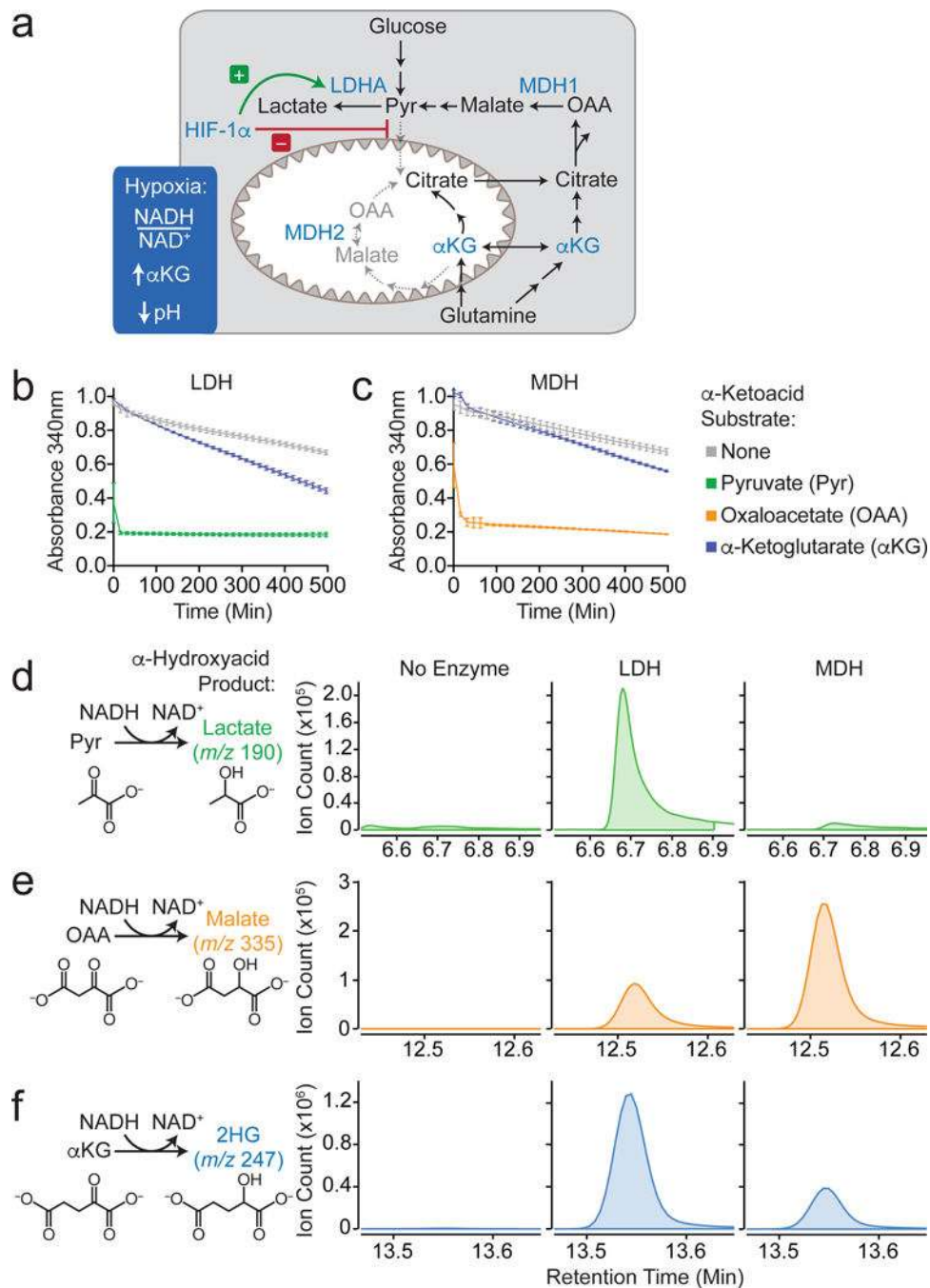


Figure 1. LDH and MDH enzymes catalyze reduction of the alternative substrate α KG
(a) Schematic of metabolic changes that occur in hypoxic cells. LDHA, MDH1, and MDH2 represent potential enzymatic sources of L-2HG production in cells. **(b)** Enzyme assay measuring NADH consumption by LDH purified from bovine heart (5 units/ml) in reactions with either no substrate (grey), pyruvate 0.3 mM (green), or α KG 1 mM (blue). **(c)** NADH consumption by MDH purified from porcine heart (5 units/ml) in reactions with either no substrate (grey), OAA 0.3 mM (orange), or α KG 3 mM (blue). Data in **b** and **c** are mean \pm 95% c.i. for triplicate reactions. **(d–f)** Alpha-hydroxyacid product formation catalyzed by

dehydrogenases. GC-MS analysis of **(d)** lactate production from pyruvate, **(e)** malate production from oxaloacetate, or **(f)** 2HG production from α .KG in 6 hr enzyme reactions with either no enzyme, LDH purified from bovine heart (10 μ g/ml), or MDH purified from porcine heart (10 μ g/ml). Reactions were conducted in potassium phosphate buffer 33 mM, pH 7.0, with NADH 0.22 mM. Results throughout figure are representative of ≥ 3 independent experiments.

Author Manuscript

Author Manuscript

Author Manuscript

Author Manuscript

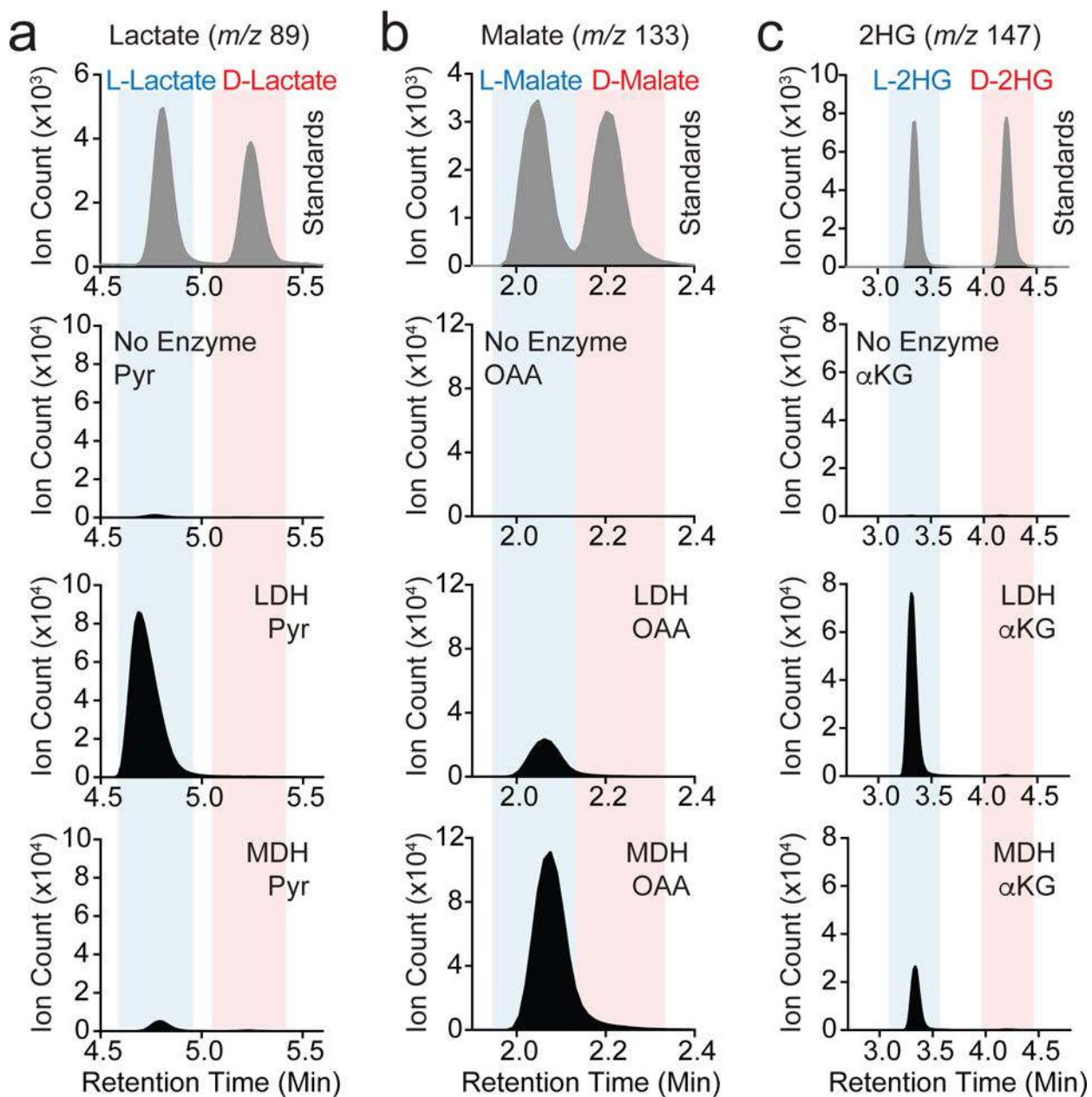


Figure 2. LDH and MDH selectively produce L- α -hydroxyacids, including L-2HG
 (a–c) Chiral LC-MS analysis resolving enantiomers of (a) lactate produced from pyruvate, (b) malate produced from oxaloacetate, or (c) 2HG produced from α KG in 6 hr reactions with either no enzyme, LDH purified from bovine heart (5 units/ml), or MDH purified from porcine heart (5 units/ml) in potassium phosphate buffer 33 mM, pH 7.0, with NADH 0.22 mM and 1 mM substrate. The top panels show mixtures of standards for L- and D-lactate, malate, and 2HG that were derivatized and analyzed by the same method in parallel. Vertical blue and red bars in background serve as visual references to facilitate identification of L- and D- enantiomers, respectively. Results throughout figure are representative of ≥ 3 independent experiments.

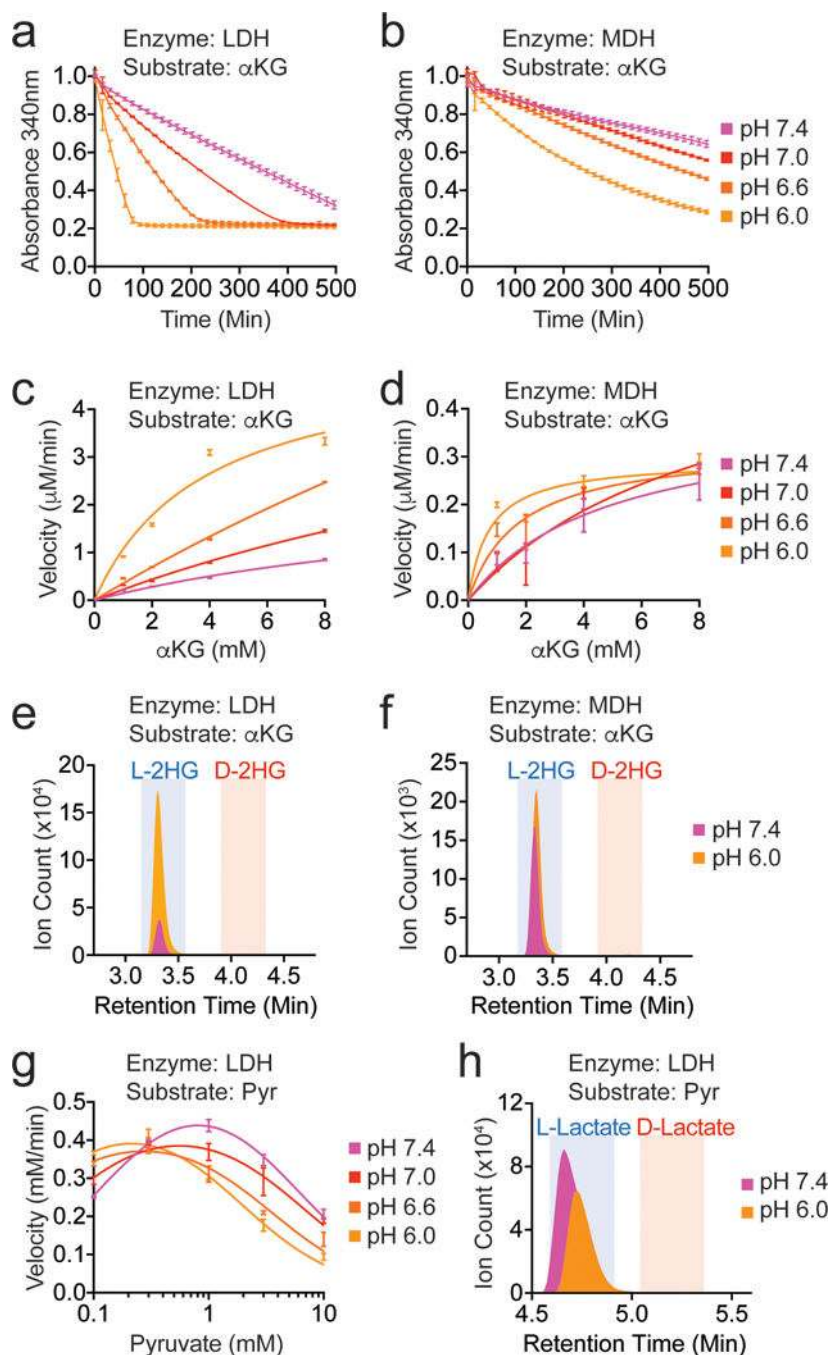


Figure 3. Acidic pH enhances L-2HG production by LDH and MDH

(a, b) Increased rates of NADH consumption in acidic reaction conditions with purified (a) LDH or (b) MDH at 5 units/ml and α KG 3 mM. Data for a and b are mean \pm 95% c.i. for triplicate reactions. (c, d) Reaction velocities as a function of α KG concentration for purified (c) LDH or (d) MDH at 5 units/ml. (e, f) Chiral LC-MS analysis of 2HG enantiomers from 6 hr reactions with purified (e) LDH or (f) MDH at 5 units/ml and α KG 1 mM. (g) Reaction velocities as a function of pyruvate concentration for purified LDH at 1 μ g/ml. (h) Chiral LC-MS analysis of lactate enantiomers from 6 hr reactions with purified

LDH at 5 units/ml and pyruvate 1 mM. Reactions were in potassium phosphate buffer 33 mM at indicated pH with NADH 0.22 mM. Data for **c**, **d**, and **g** are mean \pm s.d. for triplicate reactions. Results throughout figure are representative of ≥ 3 independent experiments.

Author Manuscript

Author Manuscript

Author Manuscript

Author Manuscript

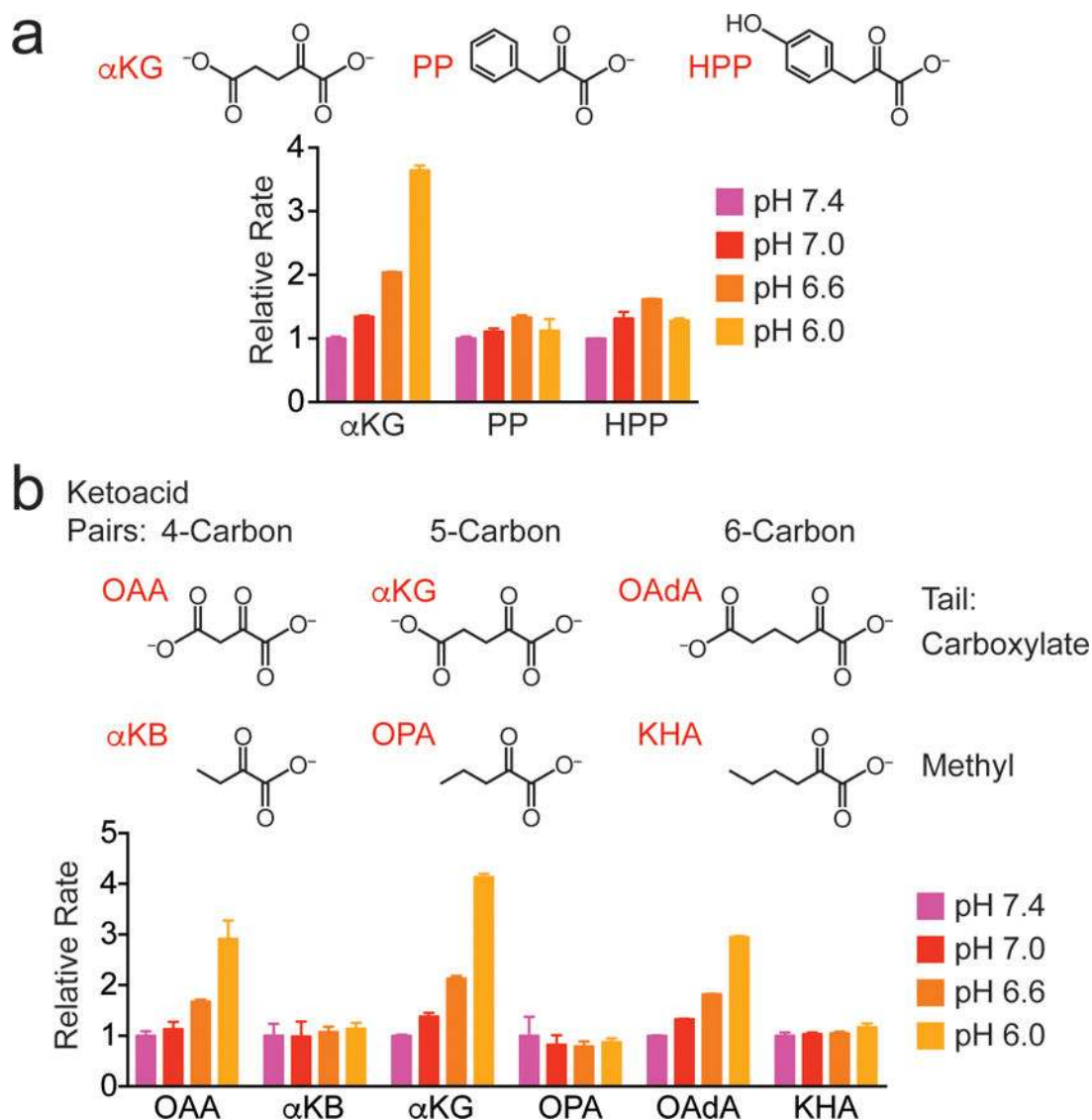


Figure 4. LDH exhibits pH-sensitive reduction of alpha-ketoacids with carboxylate tails
(a) Relative rates of NADH consumption at indicated pH with purified LDH 5 units/ml, NADH 0.22 mM, and substrate 1 mM. For each substrate, the rate at pH 7.4 was normalized to 1 to illustrate degree of rate enhancement with acidification. Structures for substrates alpha-ketoglutarate (α KG), phenylpyruvate (PP), and hydroxyphenylpyruvate (HPP). **(b)** Relative rates of NADH consumption at indicated pH with purified LDH 5 units/ml, NADH 0.22 mM, and substrate 1 mM. For each substrate, the rate at pH 7.4 was normalized to 1 to illustrate degree of rate enhancement with acidification. Structures for alpha-ketoacid substrates with carboxylate tails, oxaloacetate (OAA), α KG, oxoadipic acid (OAdA) along with their respective methylated counterparts alpha-ketobutyrate (α KB), oxopentanoic acid (OPA), and ketohexanoic acid (KHA). Data are mean \pm s.d. for triplicate reactions. Results throughout figure are representative of ≥ 3 independent experiments.

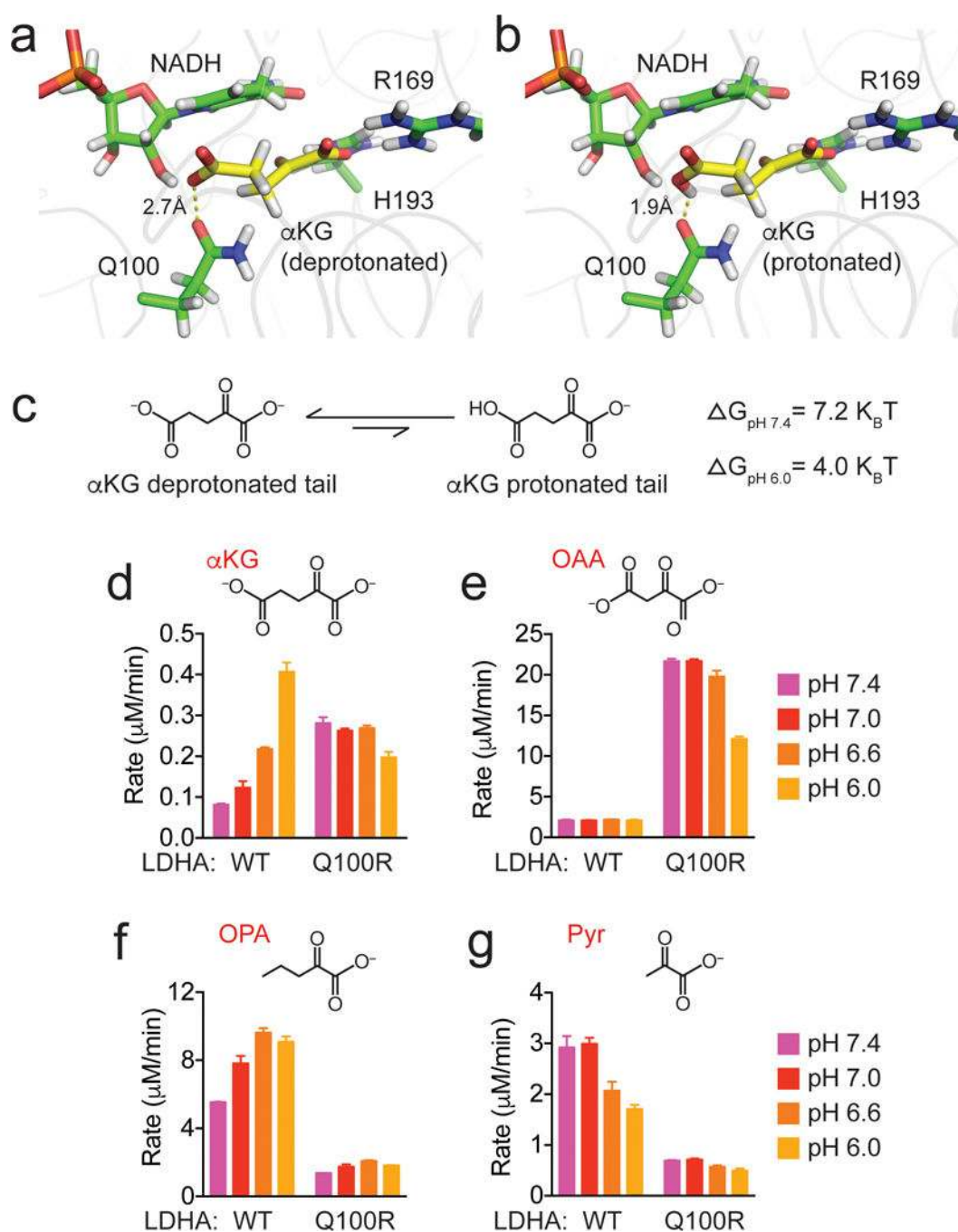


Figure 5. Acidity-induced rate enhancement arises from preference of LDHA for protonated form of αKG

(a) Virtually docked structure of deprotonated αKG (yellow) bound to LDHA, showing a potentially unfavorable interaction between the carbonyl of the Q100 residue, and the tail of αKG . (b) Virtually docked structure of protonated αKG (yellow) bound to LDHA, showing a potential hydrogen-bond interaction between the carbonyl of the Q100 residue, and the protonated carboxylate tail of αKG , predicted to be the dominant bound species by Monte Carlo simulations. (c) The equilibrium of protonation states of the tail of αKG in solution.

Shown on the right is the theoretical free energy penalty of protonating the tail at pH 7.4 ($\Delta G_{pH\ 7.4}$) and pH 6.0 ($\Delta G_{pH\ 6.0}$) in units of $k_B T$ where k_B is the Boltzmann constant and T is the absolute temperature. **(d–f, g)** Wildtype (WT) or mutant (Q100R) LDHA enzymes were purified and used in enzymatic reactions with **(d)** alpha-ketoglutarate (α KG), **(e)** oxaloacetate (OAA), **(f)** oxopentanoic acid (OPA), or **(g)** pyruvate (Pyr). Reactions were performed in potassium phosphate buffer 33 mM at the indicated pH, NADH 0.22 mM, 1 mM substrate, and enzyme at **(d, f)** 7 μ g/ml, **(e)** 0.7 μ g/ml, or **(g)** 0.07 μ g/ml. Data for **d–g** are mean \pm s.d. for triplicate reactions. Results throughout figure are representative of ≥ 3 independent experiments.

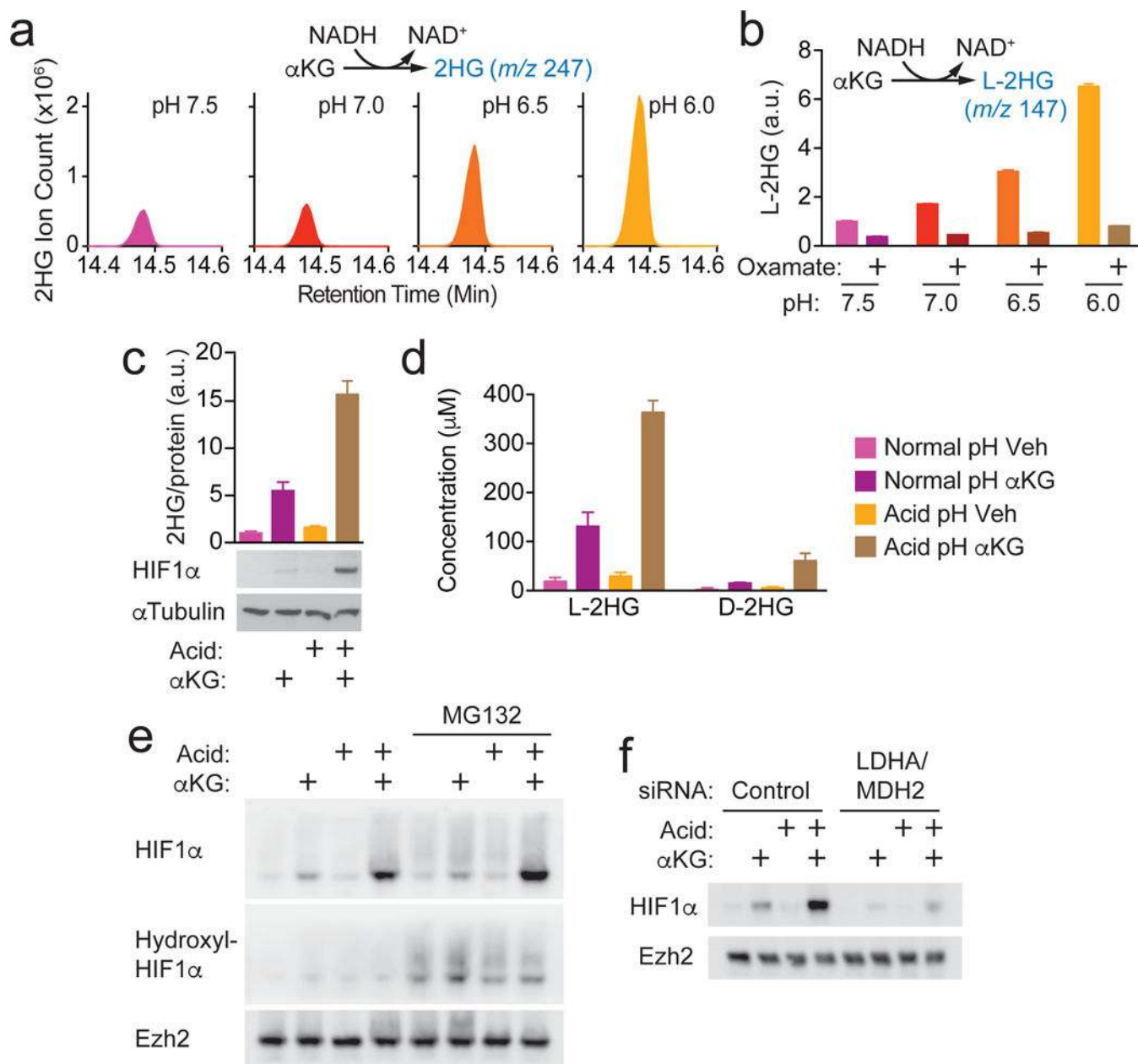


Figure 6. Acid-enhanced production of L-2HG stabilizes HIF-1 α

(a) SFXL cells were lysed in non-denaturing conditions at indicated pH. Cell lysates were incubated for 16 hr with α KG 1 mM and NADH 0.22 mM. Total 2HG was analyzed by GC-MS. (b) Lysate reactions were prepared as in a with addition of either vehicle or oxamate 1 mM. L-2HG was measured by chiral LC-MS. Data are mean \pm s.d. for triplicate reactions. (c) SFXL cells were cultured for 24 hr in standard DMEM or DMEM titrated to pH 6.0 ('acid') with vehicle or cell-permeable dimethyl- α KG 5 mM. Total 2HG was measured by GC-MS. Data are mean \pm s.d. for triplicate wells. (d) Quantification of intracellular L- and D-2HG concentrations by LC-MS (see Online Methods). Data are mean \pm s.d. of a total of 6 replicates per condition from 2 independent experiments. (e) 293T cells were cultured for 24 hr as in c with addition of vehicle or MG132 10 μ M for the final 1 hr. Western blotting of

nuclear extracts shows HIF-1 α , hydroxyl-HIF-1 α , and Ezh2 (loading control). **(f)** LDHA and MDH2 were targeted by siRNAs in SFXL cells followed by culture for 24 hr as in **c**. Western blot for **c** used whole cell lysates, while **e** and **f** used nuclear extracts. Full blot images for **c**, **e** and **f** are shown in Supplementary Fig. 11. Results for **a–c** and **e** are representative of ≥ 3 independent experiments. Results for **f** are representative of 2 independent experiments.

Author Manuscript

Author Manuscript

Author Manuscript

Author Manuscript